Langmuir

Article

pubs.acs.org/Langmuir

Homeotropic Alignment of Lyotropic Chromonic Liquid Crystals Using Noncovalent Interactions

Joonwoo Jeong,*[,†] Ganghee Han,[†] A. T. Charlie Johnson,[†] Peter J. Collings,[†,‡] Tom C. Lubensky,[†] and Arjun G. Yodh[†]

[†]Department of Physics and Astronomy, University of Pennsylvania, Philadelphia, Pennsylvania 19104, United States

[‡]Department of Physics and Astronomy, Swarthmore College, Swarthmore, Pennsylvania 19081, United States

Supporting Information

ABSTRACT: We report on the homeotropic alignment of lyotropic chromonic liquid crystals (LCLCs). Homeotropic anchoring of LCLCs is difficult to achieve, and this challenge has limited development of applications for LCLCs. In this work, homeotropic alignment is achieved using noncovalent interactions between the LCLC molecules and various alignment layers including graphene, parylene films, poly(methyl methacrylate) films, and fluoropolymer films. The LCLC molecules are unique in that they self-assemble via noncovalent interactions in water into elongated aggregates which, in turn, form nematic and columnar liquid crystal (LC) phases. Here we exploit these same noncovalent interactions to induce homeotropic anchoring of the nematic LCLC. Homeotropic alignment is confirmed by polarized optical microscopy and conoscopy. We also report on novel transient stripe textures that occur when an initial flow-induced planar alignment transforms into the equilibrium homeotropic alignment required by boundary conditions. An understanding of this behavior could be important for switching applications.

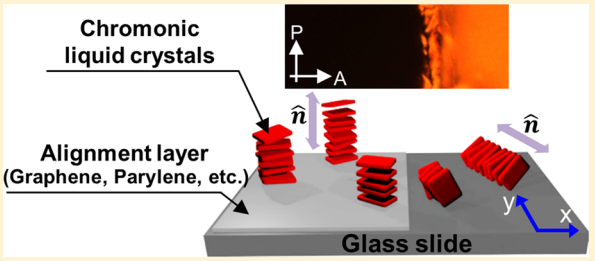

INTRODUCTION

Lyotropic chromonic liquid crystals (LCLCs) are composed of molecules in water that self-assemble into elongated aggregates, and these aggregates, in turn, form nematic or columnar LC phases that depend on temperature and chromophile concentration.[1−5] Such aqueous LCLC phases arise in solutions of dyes, drugs, nucleotides, and DNA, and they are under investigation for a variety of water-based applications.[6−23] Most LCLC molecules have a plank-like shape composed of polyaromatic cores and peripheral polar groups that are usually ionic. Thus, noncovalent intermolecular interactions, including electrostatic forces between ionized polar groups, $\pi-\pi$ stacking, van der Waals interaction, and hydrophobic interactions between aromatic cores, cause the molecules to stack like poker chips and make elongated aggregates. The aggregates are flexible, typically with scission energies in the 7−11 k_BT range.[10,24,25] The aggregates also interact to form nematic and columnar phases via excluded-volume, electrostatic, and hydration interaggregate forces. Together, these intra- and interaggregate interactions determine LCLC phase behavior, elasticity,[26,27] and other properties whose potential applications are actively investigated.[21,28,29]

Generally, the director configuration of a LC sample is determined by a balance between bulk elasticity and surface anchoring. Surface anchoring, in particular, plays a crucial role in the applications of thermotropic LCs.[30] However, little is known about the surface anchoring of LCLCs and how to control it,[5,31−36] *especially homeotropic anchoring* at interfaces wherein the LC director is perpendicular to the surface. It is known that homeotropic anchoring of LCLCs is difficult to achieve; most surfaces, including glass, give rise to planar anchoring, and the usual surface treatments for homeotropic anchoring of thermotropic LCs do not work for LCLCs.[35,36] In fact, many suggested applications of LCLCs that utilize their anisotropic optical and electric properties are limited by a lack of control of surface anchoring.

In this investigation, we utilize noncovalent interactions between the nematic LCLCs and alignment layers to achieve homeotropic anchoring. Specifically, we develop alignment layers based on graphene, parylene films, poly(methyl methacrylate) (PMMA) films, and fluoropolymer films for homeotropic anchoring of two well-known LCLCs: disodium cromoglycate (DSCG) and Sunset Yellow FCF (SSY). Exploration of hydrophobic fluoropolymer films was inspired by previously reported experiments employing PDMS films.[35,36] Following this work, we also tested moderately hydrophobic films such as PMMA. Finally, our use of graphene layers and paralyene films was based on expectations about the potential for $\pi-\pi$ stacking of organic molecules with aromatic rings. This newfound ability to create homeotropic alignment also enables us to initiate and investigate some novel dynamic LCLC phenomenology. In particular, we report on transient stripe textures that develop when an initial flow-induced planar alignment transforms into the equilibrium homeotropic align-

Received: December 20, 2013
Revised: February 20, 2014
Published: February 23, 2014

   dx.doi.org/10.1021/la404893t | *Langmuir* 2014, 30, 2914−2920

ment required by the boundary conditions of the sample cell surfaces. This remarkable texture appears to be a metastable configuration in which large stresses, resulting from the initial alignment and the boundary condition, are relaxed by twist deformations. Ultimately, these texture dynamics could be important in switching applications of LCLCs using homeotropic alignment layers.

EXPERIMENTAL SECTION

Preparation of Alignment Layers. Graphene grown by chemical vapor deposition (CVD) on a copper foil was transferred to a glass substrate. The copper foil (Alfa Aesar, 46365) was placed in a tube furnace (4 in. diameter) heated to 1020 °C with 80 sccm of H_2 gas (600 mTorr, temperature increasing rate is 17 °C/min). For graphene growth, 45 sccm of CH_4 gas was added (1000 mTorr) for 65 min. After the cooling process, the graphene/copper foil was cut into pieces (20 × 20 mm), and the graphene was transferred by a bubbling transfer technique with 0.1 M KOH solution onto a glass substrate.[37] To prevent delamination of graphene from the glass in contact with aqueous LCLC, the surface of the glass substrate was treated by hexamethyldisilazane (HMDS) vapor for 30 min before transferring the graphene.

Parylene-N films were directly deposited on glass substrates by CVD using a commercially available parylene coater (PDS2010, Specialty Coating Systems). 0.5−2 g of [2.2]paracyclophane was deposited under vacuum conditions (~55 mTorr) onto precleaned glass slides and glass capillaries without any surface treatment. Temperatures used for vaporization, pyrolysis, and deposition of parylene-N were 160 °C, 650 °C, and room temperature, respectively.

For fluoropolymer films, 100 μL of coating solution (Novec 1700, 3M) was spin-cast onto a precleaned glass coverslip (25 × 25 mm) at 5000 rpm for 1 min. For poly(methyl methacrylate) (PMMA) films, 1 mL of coating solution (950PMMA C2, MicroChem) was spin-cast onto a precleaned glass slide at 3000 rpm for 1 min. Then, PMMA films were baked at 150 °C for 2 min on a hot plate.

Preparation of Sample Cells. Disodium cromoglycate (DSCG) and Sunset Yellow FCF (SSY) were purchased from Sigma-Aldrich at purities of >95% and 90%, respectively. DSCG was used as received, and SSY was purified using a precipitation method.[10,15,24] We dissolved each compound into deionized water (18.2 MΩ·cm) to make DSCG (15.0 wt %) and SSY (31.0 wt %) solutions in the nematic phase. The vacuum suction method was performed to fill the interior of parylene-coated capillaries. A drop of the nematic LC was sandwiched with 20 μm spacers by two substrates on which the alignment layers were coated. LCLC samples were sealed with epoxy glue to prevent evaporation of water. Then, all samples were observed immediately after preparation at an ambient temperature of 23 °C without temperature change.

Optical Microscopy. We collected bright-field, polarized optical microscopy (POM) images using an inverted microscope (DM IRB, Leica) with a 10× dry objective. For the conoscopy image, we employed a 63× (N.A. = 0.7) dry objective with a coverslip-thickness correction. The samples were rotated on a circular stage located between a polarizer and an analyzer. Most images were taken with a color CCD camera (UC-1800DS-CL, UNIQ Vision Inc.) under polychromatic illumination derived from a halogen lamp. For the quasi-monochromatic illumination measurements (center wavelength = 650 nm, fwhm = 10 nm), we employed a black-and-white CCD camera (UP-680CL, UNIQ Vision Inc.) and a bandpass filter (P10-650, Orion).

Contact Angle Measurement. Static contact angles of sessile water or LCLC droplets on alignment layers were measured using an optical tensiometer (Attension Theta, Biolin Scientific). Briefly, 0.5−1 μL of a solution was placed by a pipet onto a substrate on which an alignment layer was coated. Drop shapes were fit to the Laplace−Young equation by image analysis software (CAM Series Software, KSV Instruments Ltd.), and the shape symmetry of the sessile droplets was confirmed in all measurements. In order to minimize droplet evaporation, all measurements were conducted at ambient temperature and within 30 s after placing the droplets on the alignment layer.

RESULTS AND DISCUSSION

Homeotropic Alignment of LCLCs. Homeotropic alignment of the LCLCs on the alignment layers was confirmed by polarized optical microscopy (POM) and conoscopy.[35,36] Figure 1a shows the top view of the nematic DSCG sandwiched between two graphene-coated glass surfaces. Figure 1b was taken with nematic SSY sandwiched between two parylene-coated glass surfaces. This configuration of LCLCs sandwiched between two alignment layers (graphene layers or parylene films) showed no transmission under crossed polarizers (polarizer directions are shown as white arrows). As sketched on the left side of Figure 1c, this behavior arises because the director ($\hat{n}$) of the LCLC aggregates is oriented perpendicular to the substrates. In other words, the nematic LCLCs have homeotropic anchoring on the alignment layers. By contrast, in the bright regions of Figure 1a,b wherein nematic LCLCs are in contact with bare glass substrates, the LC directors have nonzero components parallel to the substrates owing to degenerate planar anchoring (see right side of Figure 1c). Thus, the transmittance of these regions varies as the sample is rotated. In Figure 1a, cracks and holes of graphene appear as bright regions because they expose glass substrates.

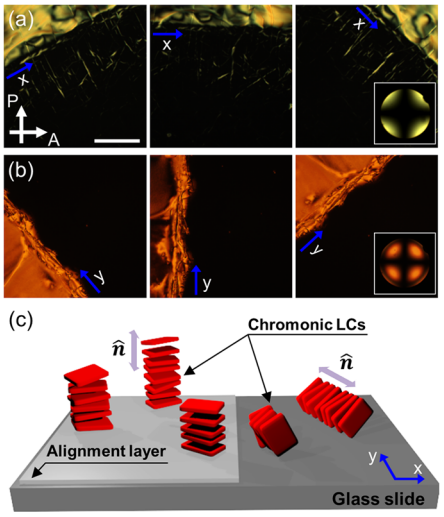

Figure 1. Polarized optical microscopy images of (a) DSCG sandwiched between two graphene-coated glass surfaces and (b) SSY sandwiched between two parylene-coated glass surfaces. The white arrows indicate pass axis directions of the input polarizer (P) and the analyzer (A). The blue arrows represent the *x*-axis (*y*-axis) of each sample which is rotated. Scale bar is 200 μm. In the bright regions, the bare glass substrates are exposed; in the dark regions, the LCLC is sandwiched by the alignment layer-coated glass substrates. The insets at the right bottom of each figure show conoscopy images of the dark regions; their patterns were constant as a function of rotation angle. (c) A schematic diagram of the anchoring of LCLCs on a glass slide and an alignment layer. Stacks of plank-like molecules represent LCLC aggregates, and double-headed arrows indicate LC directors ($\hat{n}$). The LCLCs show homeotropic anchoring on the alignment layer and planar anchoring on the bare glass slide.

The insets in Figure 1a,b show conoscopic images of each homeotropic region. This cross shape is observed in the conoscopy of a uniaxial crystal along the crystal axis and indicates homeotropic alignment. The same procedure was

dx.doi.org/10.1021/la404893t | Langmuir 2014, 30, 2914−2920

employed to confirm that nematic SSY has homeotropic alignment on fluoropolymer and PMMA films. Interestingly, only graphene induced homeotropic alignment of both DSCG and SSY; the other films did not induce homeotropic alignment of DSCG.

The stability of the homeotropic alignment as a function of temperature and time was also checked. The samples recovered their homeotropic alignment after they were heated through the isotropic−nematic transition and then cooled to ambient temperature. When significant evaporation of water from the samples occurred, the resultant samples exhibited a phase transition from the nematic to the columnar phase. In the process, the samples lost their homeotropic alignment and exhibited characteristic textures of the columnar LCLC phase.[35] We did not observe substantial changes in homeotropic alignment except when this nematic−columnar phase transition occurred.

In the case of parylene and PMMA films, we observed a slow anchoring transition.[33] Although uniform homeotropic alignment was achieved initially over a large area, some regions of planar alignment appeared on the films slowly, over a period of several weeks.

The molecular forces responsible for homeotropic anchoring of LCLCs on alignment layers are noncovalent interactions which can vary depending on the alignment layer surface chemistry. For example, the homeotropic alignment of LCLCs has been reported on very hydrophobic surfaces.[35,36] Indeed, in our experiments with SSY on fluoropolymer and parylene alignment layers, a hydrophobic interaction appears to facilitate homeotropic anchoring. The fluoropolymer and the parylene films are clearly hydrophobic; the contact angles of deionized water on these films were ∼105° and ∼90°, respectively. Further, the LCLC SSY exhibited homeotropic anchoring even on moderately hydrophobic alignment layers such as the PMMA film and the graphene layer, on which the contact angles of deionized water were ∼70° and ∼80°, respectively.

In the case of DSCG, however, even the highly hydrophobic fluoropolymer film did not induce homeotropic alignment. This observation suggests that the homeotropic anchoring strength of DSCG is weaker than SSY, though it is still large enough to facilitate transient and weak homeotropic anchoring on hydrophobic silane-treated substrates.[33] (Note: at a later time, this system exhibited an anchoring transition from homeotropic to planar anchoring.[33]) We hypothesize that the more flexible linkage between the aromatic rings of DSCG compared to SSY[2,9,15] decreases interactions with the alignment layer and thus diminishes the chance for homeotropic anchoring on the substrates we have studied.

In the case of the graphene layer, homeotropic alignment of the LCLCs may arise from other effects in addition to the hydrophobic interaction. The graphene layer, for example, induced homeotropic alignment of DSCG while the other more hydrophobic films did not. Therefore, $\pi-\pi$ stacking is one candidate that could play a role facilitating homeotropic anchoring of LCLCs on graphene.[38,39] Specifically, it is possible that $\pi-\pi$ stacking[10,23] between polyaromatic cores of the LCLC molecules and the hexagons of graphene, could initiate formation of face-to-face stacks of plank-like LCLC molecules on graphene. Over the years, such $\pi-\pi$ stacking between organic molecules and allotropes of carbon such as fullerenes, carbon nanotubes, and graphene has been observed.[40−48] According to this argument, $\pi-\pi$ stacking should also be present in the parylene films,[49] but it appears that such stacking effects are not sufficient to induce homeotropic anchoring of DSCG. Finally, it is possible that van der Waals interaction between the aromatic rings facing one another can also lead to homeotropic alignment.[38,39] However, these ideas for the interactions responsible for homeotropic alignment are not resolved in the scientific community; for example, in thread-like models[18] that assume side-by-side stacking instead of face-to-face stacking of the molecules, both $\pi-\pi$ stacking and the van der Waals interactions should not lead to homeotropic anchoring.

Observation of Transient Stripe Textures. The ability to achieve homeotropic anchoring of LCLCs enables us to probe the dynamical behavior of LCLCs as they evolve toward equilibrium configurations imposed by boundary conditions. For instance, Figure 2 shows the evolution of nematic SSY sandwiched between two parylene-coated substrates. These evolving textures are unusual, in part as a result of the LCLC's elastic anisotropy, and interesting from a fundamental viewpoint; furthermore, transient stripe textures provide useful information about the relationship between flow and surface anchoring that aids in the characterization of basic LCLC properties such as anchoring strength and the magnitude of anisotropic viscosities. From an applied perspective, transient stripe textures can be a serious time-response issue in applications involving alignment and switching of LCLCs; for example, since the stripe textures precede homeotropic alignment and disappear slowly, the preparation and recovery of aligned LCLCs are slow.

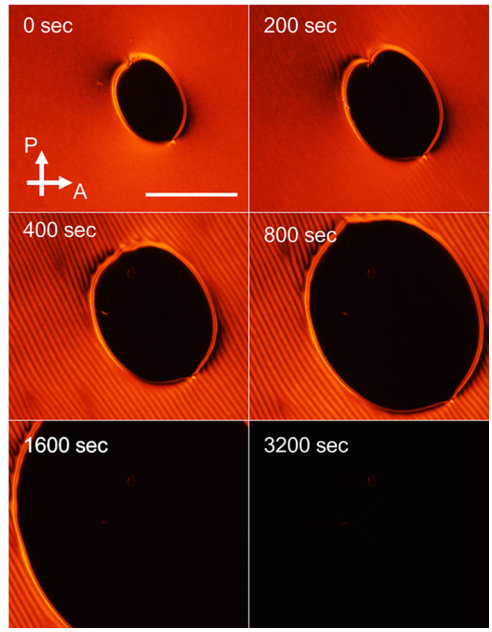

Figure 2. A time sequence of polarized optical microscopy images of initially planar-aligned SSY sandwiched between two parylene-coated glasses. The white arrows represent the pass axis directions of the input polarizer (P) and the analyzer (A). The 0 s image of the time sequence corresponds to when the observations started. Scale bar is 200 μm. The growing dark region has homeotropic alignment. Notice that after 200 s the stripe texture starts to become visible outside the top and bottom of the homeotropic domains and becomes more apparent thereafter.

In Figure 2, we show transient stripe textures observed when an initial planar alignment induced by flow transforms into

dx.doi.org/10.1021/la404893t | Langmuir 2014, 30, 2914−2920

homeotropic alignment forced by the alignment layer. Briefly, in the course of preparing the cell, in which a nematic sessile droplet is sandwiched between substrates, the initial director configuration aligns mostly parallel to the substrate due to spreading-induced flow. Figure 2 shows a sequence of POM images of an SSY sandwich cell as a function of time; at 0 s, we see the initial planar alignment, except for a small homeotropic domain at the center. After several minutes (200 s in Figure 2), the planar alignment starts to develop stripe textures, and after several tens of minutes the stripes are replaced by a full homeotropically aligned domain. Below, we show a collection of clues that lead us to an understanding of the textures.

First, we observe that the stripes are approximately parallel to the direction of the initial planar alignment in the capillary whose cross section is shown in Figure 3a. As shown in Figure 3b, the parylene-coated capillary induces homeotropic alignment of SSY except in the region around the side wall of the capillary. Initially, flow-induced planar alignment of the nematic LCLC is parallel to the direction of flow, excepting the regions near the side wall. Then, as shown in Figure 3c,d, the planar alignment develops a stripe texture that is mostly parallel to the capillary axis. The stripe texture was also observed in thick capillaries up to 100 μm in thickness, and the stripe period increased when the cell thickness increased in a wedge cell (see Supporting Information). Eventually, the stripe texture is replaced by the homeotropic alignment (Figure 3b).

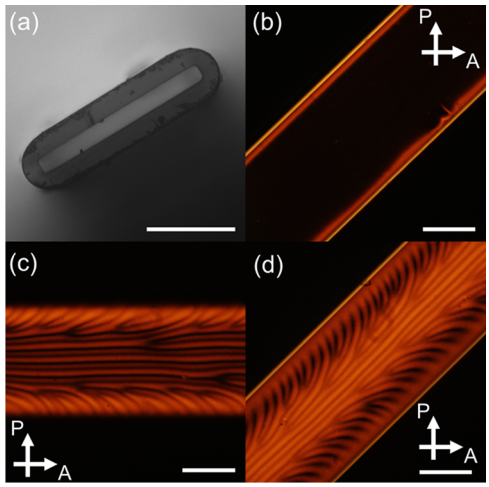

Figure 3. SSY confined in a parylene-coated capillary with a rectangular cross section. Scale bar is 200 μm. (a) Cross section of the capillary. (b) Polarized optical microscopy images of SSY confined in the parylene-coated capillary. White arrows correspond to the directions of the input polarizer (P) and the analyzer (A). The dark region at the sample center is the homeotropic region of SSY, and the bright regions are distorted configurations of SSY near the side wall of the capillary. (c, d) Polarized optical microscopy images of the transient stripe texture observed before homeotropic alignment is achieved. Note that the stripes are almost parallel to the capillary axis except those in the region around the side wall.

To better understand the structure of the stripe texture, we investigated it further under various polarizer, analyzer, and wave plate axis directions. In Figure 4, all images were taken from the same region (yellow boxes), and the white arrows (polarizer and analyzer) and yellow arrows (the fast axis of wave plate) correspond to different axis directions of the optical components. Quasi-monochromatic illumination at a wavelength of 650 nm was used for these images of the middle region between top/bottom substrates. Without polarizers, or with only one polarizer (analyzer), the stripes were not observed. Figure 4a,b shows that bright stripes experienced intensity changes due to rotation of the crossed polarizers. But, the bright stripes showed no extinction with the crossed polarizers, and the dark stripes did not get brighter. On the other hand, with the parallel polarizers in Figure 4c–e, dark stripes in the crossed polarizer configuration become bright, while bright stripes in the crossed polarizer configuration become dark. In addition, with the wave plate (2π retardation at 550 nm) and the crossed polarizers, the stripes exhibited various patterns shown in Figure 4f–i.

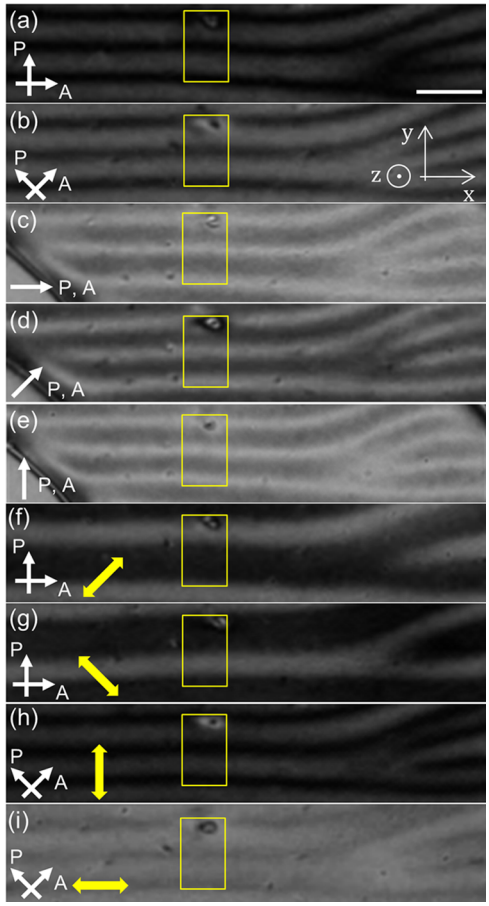

Figure 4. Optical microscopy images of the stripe texture under quasi-monochromatic illumination (center wavelength = 650 nm) with polarizers and a wave plate. The yellow boxes enclose the same region. White arrows represent the directions of the input polarizer (P) and the analyzer (A), and the yellow arrows represent the direction of the wave plate's fast axis. Scale bar is 50 μm.

On the basis of these observations and the expectation of homeotropic anchoring at the boundary, we suggest a LC director configuration for these metastable stripes. As shown in Figure 5, the key feature in the stripe configuration is a twist along the z-direction, which is perpendicular to the sample plane. This twist is modulated along the direction perpendicular to the stripes. In Figure 4a,b, the bright stripes change their intensity, but they are never extinguished under the rotation of the crossed polarizer. This implies that the directions of planar components of the LC directors in the bright stripes change along the z-direction (the second and fourth columns from the left in Figure 5). By contrast, the dark stripes hardly change in their intensity, which implies that these stripes do not have

dx.doi.org/10.1021/la404893t | Langmuir 2014, 30, 2914–2920

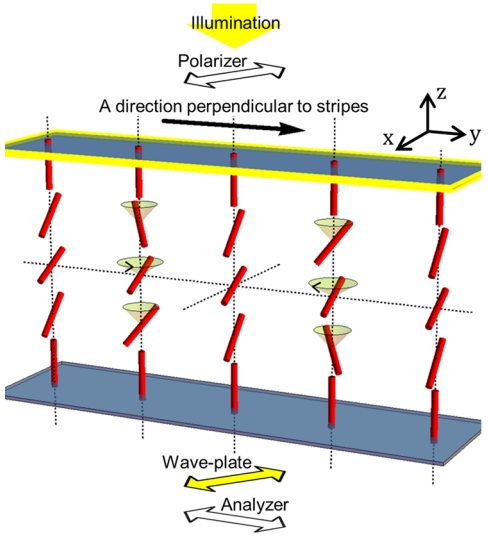

Figure 5. Schematic diagram of the suggested LC director configuration of the stripes. Nematic LCLC is sandwiched between top/bottom plates coated by a homeotropic alignment layer. A black straight arrow shows a direction perpendicular to stripes. A yellow box around the top plate corresponds to the yellow box in Figure 4. Red rods represent LC directors that have homeotropic anchoring at top and bottom alignment layers. Cones and rotating arrows highlight the regions with twists of different handedness. Each double-headed arrow represents the pass axis (fast axis) direction of the input/output polarizers (wave plate).

twist and the directors are mostly perpendicular to the sample plane (the first, third, and fifth columns from the left in Figure 5). This model is also consistent with observations in Figure 4c–e using parallel polarizers. Lastly, in Figure 4f,g, a wave plate reveals the difference between two adjacent bright stripes in the yellow box; the handedness of the twist deformation in each adjacent stripe is opposite (the cones and rotating arrows in Figure 5). Jones matrix-simulated POM images based on the configuration shown in Figure 5 exhibited good agreement with the experiments shown in Figure 4 (see Supporting Information).

The key to this transient stripe behavior is the ease with which LCLCs can twist. The flow-induced planar alignment and the homeotropic anchoring at the top and bottom substrates lead to large bend and splay deformation, and because the elastic modulus of twist deformation is an order of magnitude smaller than the moduli of splay and bend deformation,[26,27] it is natural for the LCLCs to acquire a twist deformation that eventually relaxes the large bend and splay deformation caused by the boundary conditions. Interestingly, the proposed scheme is similar to reports of pattern formation resulting from large elastic anisotropy in thermotropic nematic LCs.[50−57] Especially, in refs 50 and 51, although there are external fields and the boundary conditions are different, the configuration is quite similar to ours because there is twist along the *z*-direction and the handedness of the twist changes periodically. It may be relevant to patterns observed in sheared polymeric (thermotropic) nematic LCs, which also have a very small twist modulus.[55,56]

Lastly, it is worth emphasizing that the stripes always follow the flow-induced planar alignment, in which the bulk director is mostly planar and form well before the formation of the homeotropic state. It should be noted that this transition to stripes is different from the transition in ref 54, where the stripes appear from an almost homeotropic alignment. The texture evolution involving stripes was observed in temperature experiments as well as during preparation of the sandwich-cell/capillary samples. During heating the LCLC sample usually experiences a thermal expansion-induced flow, probably because of nonuniform heating. As a result, the regular stripe structure was destroyed by the flow when the sample was heated. Cooling to room temperature recovered the stripe textures, but the previous pattern was not exactly reproduced because the flow direction was different. Clearly, further investigation of the possible instability mechanisms is needed.

CONCLUSION

In summary, we demonstrate homeotropic alignment of two well-known nematic LCLCs using graphene, parylene films, PMMA films, and fluoropolymer films as alignment layers. It has been difficult to achieve homeotropic anchoring of LCLCs, and this difficulty in the control of surface anchoring has limited many suggested applications of LCLCs. Our experiments suggest that this homeotropic anchoring may arise from noncovalent interactions, e.g., hydrophobic interactions, $\pi-\pi$ stacking, and van der Waals interactions between the LCLC molecules and the alignment layers. Understanding and characterizing the interactions responsible for anchoring of nematic/columnar LCLCs will be essential for applications of LCLCs. In addition, new applications of LCLCs can now utilize the excellent properties of these alignment layers, e.g., the high electrical conductivity of graphene and chemical inertness of parylene.

We also report on transient stripe textures that occurred while LCLCs having a planar initial alignment transform into the equilibrium homeotropic alignment. Based on the optical observations and the unusually small twist modulus of LCLCs, a fascinating director configuration of the stripe texture is proposed with a twist deformation along the *z*-direction and with twist modulation along the direction perpendicular to the stripes. Understanding these effects could lead to improved usage of LCLCs in switching and alignment applications. For instance, by utilizing the negative $\Delta\chi$ $(= \chi_{\parallel} - \chi_{\perp})$ of LCLCs, wherein $\chi_{\parallel}$ is the diamagnetic susceptibility measured parallel to the director and $\chi_{\perp}$ is its orthogonal counterpart, magnetic fields can stabilize and control stripe textures for optical applications[55,58] or expedite homeotropic alignment.

ASSOCIATED CONTENT

Supporting Information

(1) Stripe period as a function of cell thickness and (2) comparison between the experiment and Jones matrix calculation of polarized optical microscopy images. This material is available free of charge via the Internet at http://pubs.acs.org.

AUTHOR INFORMATION

Corresponding Author

*E-mail: jjeong@sas.upenn.edu (J.J.).

Notes

The authors declare no competing financial interest.

ACKNOWLEDGMENTS

Parylene deposition was performed at the Wolf Nanofabrication Facility of the University of Pennsylvania. We thank Mohamed A. Gharbi and Kathleen J. Stebe for assistance

with the contact angle measurements, and we gratefully acknowledge financial support from the National Science Foundation through Grants DMR-1205463 and DMR-1120901 and partial support from NASA Grant NNX08AO0G.

REFERENCES

(1) Collings, P. J.; Dickinson, A. J.; Smith, E. C. Molecular aggregation and chromonic liquid crystals. *Liq. Cryst.* **2010**, *37*, 701−710.
(2) Lydon, J. Chromonic review. *J. Mater. Chem.* **2010**, *20*, 10071−10099.
(3) Lydon, J. Chromonic liquid crystalline phases. *Liq. Cryst.* **2011**, *38*, 1663−1681.
(4) Tam-Chang, S.-W.; Huang, L. Chromonic liquid crystals: properties and applications as functional materials. *Chem. Commun.* **2008**, 1957−1967.
(5) Park, H.-S.; Lavrentovich, O. D. Lyotropic Chromonic Liquid Crystals: Emerging Applications. In *Liquid Crystals Beyond Displays: Chemistry, Physics, and Applications*, Li, Q., Ed.; John Wiley & Sons: Hoboken, NJ, 2012; p 449.
(6) Hartshorne, N. H.; Woodard, G. D. Mesomorphism in the system disodium chromoglycate-water. *Mol. Cryst. Liq. Cryst.* **1973**, *23*, 343−368.
(7) Lee, H.; Labes, M. M. Cholesteric, lyotropic, and nematic phases of disodium cromoglycate in magnetic fields. *Mol. Cryst. Liq. Cryst.* **1982**, *84*, 137−157.
(8) Mariani, P.; Saturni, L. Measurement of intercolumnar forces between parallel guanosine four-stranded helices. *Biophys. J.* **1996**, *70*, 2867−2874.
(9) Nastishin, Y.; Liu, H.; Schneider, T.; Nazarenko, V.; Vasyuta, R.; Shiyanovskii, S.; Lavrentovich, O. Optical characterization of the nematic lyotropic chromonic liquid crystals: Light absorption, birefringence, and scalar order parameter. *Phys. Rev. E* **2005**, *72*, 041711.
(10) Horowitz, V.; Janowitz, L.; Modic, A.; Heiney, P.; Collings, P. Aggregation behavior and chromonic liquid crystal properties of an anionic monoazo dye. *Phys. Rev. E* **2005**, *72*, 041710.
(11) Kostko, A. F.; Cipriano, B. H.; Pinchuk, O. A.; Ziserman, L.; Anisimov, M. A.; Danino, D.; Raghavan, S. R. Salt effects on the phase behavior, structure, and rheology of chromonic liquid crystals. *J. Phys. Chem. B* **2005**, *109*, 19126−19133.
(12) Shiyanovskii, S.; Schneider, T.; Smalyukh, I.; Ishikawa, T.; Niehaus, G.; Doane, K.; Woolverton, C.; Lavrentovich, O. Real-time microbe detection based on director distortions around growing immune complexes in lyotropic chromonic liquid crystals. *Phys. Rev. E* **2005**, *71*, 020702.
(13) Shiyanovskii, S. V.; Lavrentovich, O. D.; Schneider, T.; Ishikawa, T.; Smalyukh, I. I.; Woolverton, C. J.; Niehaus, G. D.; Doane, K. J. Lyotropic chromonic liquid crystals for biological sensing applications. *Mol. Cryst. Liq. Cryst.* **2005**, *434*, 259/[587]−270/[598].
(14) Nakata, M.; Zanchetta, G.; Chapman, B. D.; Jones, C. D.; Cross, J. O.; Pindak, R.; Bellini, T.; Clark, N. A. End-to-end stacking and liquid crystal condensation of 6 to 20 base pair DNA duplexes. *Science* **2007**, *318*, 1276−1279.
(15) Edwards, D. J.; Jones, J. W.; Lozman, O.; Ormerod, A. P.; Sintyureva, M.; Tiddy, G. J. T. Chromonic liquid crystal formation by Edicol Sunset Yellow. *J. Phys. Chem. B* **2008**, *112*, 14628−14636.
(16) Park, H.-S.; Agarwal, A.; Kotov, N. A.; Lavrentovich, O. D. Controllable side-by-side and end-to-end assembly of Au nanorods by lyotropic chromonic materials. *Langmuir* **2008**, *24*, 13833−13837.
(17) Tomasik, M. R.; Collings, P. J. Aggregation behavior and chromonic liquid crystal phase of a dye derived from naphthalene-carboxylic acid. *J. Phys. Chem. B* **2008**, *112*, 9883−9889.
(18) Wu, L.; Lal, J.; Simon, K. A.; Burton, E. A.; Luk, Y.-Y. Nonamphiphilic assembly in water: polymorphic nature, thread structure, and thermodynamic incompatibility. *J, Am. Chem. Soc.* **2009**, *131*, 7430−7443.
(19) McKitterick, C. B.; Erb-Satullo, N. L.; LaRacuente, N. D.; Dickinson, A. J.; Collings, P. J. Aggregation properties of the chromonic liquid crystal benzopurpurin 4B. *J. Phys. Chem. B* **2010**, *114*, 1888−1896.
(20) Park, H.-S.; Kang, S.-W.; Tortora, L.; Kumar, S.; Lavrentovich, O. D. Condensation of self-assembled lyotropic chromonic liquid crystal sunset yellow in aqueous solutions crowded with polyethylene glycol and doped with salt. *Langmuir* **2011**, *27*, 4164−4175.
(21) Mushenheim, P. C.; Trivedi, R. R.; Tuson, H. H.; Weibel, D. B.; Abbott, N. L. Dynamic self-assembly of motile bacteria in liquid crystals. *Soft Matter* **2013**, *10*, 88−95.
(22) Bonazzi, S.; DeMorais, M. M.; Gottarelli, G.; Mariani, P.; Spada, G. P. Self-assembly and liquid crystal formation of folic acid salts. *Angew. Chem., Int. Ed. Engl.* **1993**, *32*, 248−250.
(23) Goldfarb, D.; Luz, Z.; Spielberg, N.; Zimmermann, H. Structural and orientational characteristics of the disodium/cromoglycate-water mesophases by deuterium NMR and X-ray diffraction. *Mol. Cryst. Liq. Cryst.* **1985**, *126*, 225−246.
(24) Park, H.-S.; Kang, S.-W.; Tortora, L.; Nastishin, Y.; Finotello, D.; Kumar, S.; Lavrentovich, O. D. Self-assembly of lyotropic chromonic liquid crystal Sunset Yellow and effects of ionic additives. *J. Phys. Chem. B* **2008**, *112*, 16307−16319.
(25) Renshaw, M. P.; Day, I. J. NMR characterization of the aggregation state of the azo dye sunset yellow in the isotropic phase. *J. Phys. Chem. B* **2010**, *114*, 10032−10038.
(26) Nastishin, Y. A.; Neupane, K.; Baldwin, A. R.; Lavrentovich, O. D.; Sprunt, S. Elasticity and viscosity of a lyotropic chromonic nematic studied with dynamic light scattering. 2008, arXiv:0807.2669.
(27) Zhou, S.; Nastishin, Y. A.; Omelchenko, M. M.; Tortora, L.; Nazarenko, V. G.; Boiko, O. P.; Ostapenko, T.; Hu, T.; Almasan, C. C.; Sprunt, S. N.; Gleeson, J. T.; Lavrentovich, O. D. Elasticity of lyotropic chromonic liquid crystals probed by director reorientation in a magnetic field. *Phys. Rev. Lett.* **2012**, *109*, 037801.
(28) Zhou, S.; Sokolov, A.; Lavrentovich, O. D.; Aranson, I. S. Living liquid crystals. *Proc. Natl. Acad. Sci. U. S. A.* **2014**, *111*, 1265−1270.
(29) Jeong, J.; Davidson, Z. S.; Collings, P. J.; Lubensky, T. C.; Yodh, A. G. Chiral symmetry breaking and surface faceting in chromonic liquid crystal droplets with giant elastic anisotropy. *Proc. Natl. Acad. Sci. U. S. A.* **2014**, *111*, 1742−1747.
(30) Jerome, B. Surface effects and anchoring in liquid crystals. *Rep. Prog. Phys.* **1991**, *54*, 391−451.
(31) Schneider, T.; Lavrentovich, O. D. Self-assembled monolayers and multilayered stacks of lyotropic chromonic liquid crystalline dyes with in-plane orientational order. *Langmuir* **2000**, *16*, 5227−5230.
(32) Fujiwara, T.; Ichimura, K. Surface-assisted photoalignment control of lyotropic liquid crystals. Part 2. Photopatterning of aqueous solutions of a water-soluble anti-asthmatic drug as lyotropic liquid crystals. *J. Mater. Chem.* **2002**, *12*, 3387−3391.
(33) Nazarenko, V. G.; Boiko, O. P.; Park, H.-S.; Brodyn, O. M.; Omelchenko, M. M.; Tortora, L.; Nastishin, Y. A.; Lavrentovich, O. D. Surface alignment and anchoring transitions in nematic lyotropic chromonic liquid crystal. *Phys. Rev. Lett.* **2010**, *105*, 017801.
(34) Tolkki, A.; Vuorimaa, E.; Chukharev, V.; Lemmetyinen, H.; Ihalainen, P.; Peltonen, J.; Dehm, V.; Wurthner, F. Langmuir-Schaeffer films from a π-π stacking perylenediimide dye: organization and charge transfer properties. *Langmuir* **2010**, *26*, 6630−6637.
(35) Tone, C. M.; De Santo, M. P.; Buonomenna, M. G.; Golemme, G.; Ciuchi, F. Dynamical homeotropic and planar alignments of chromonic liquid crystals. *Soft Matter* **2012**, *8*, 8478−8482.
(36) Tone, C. M.; De Santo, M. P.; Ciuchi, F. Alignment of chromonic liquid crystals: A difficult task. *Mol. Cryst. Liq. Cryst.* **2013**, *576*, 2−7.
(37) Gao, L.; Ren, W.; Xu, H.; Jin, L.; Wang, Z.; Ma, T.; Ma, L.-P.; Zhang, Z.; Fu, Q.; Peng, L.-M.; Bao, X.; Cheng, H.-M. Repeated growth and bubbling transfer of graphene with millimetre-size single-crystal grains using platinum. *Nat. Commun.* **2012**, *3*, 699.
(38) Patil, O.; Mohanty, S. Why folates self-assemble: a simulation-based study. *Mol. Simul.*, in press.

(39) Mohanty, S.; Chou, S.-H.; Brostrom, M.; Aguilera, J. Predictive modeling of self assembly of chromonics materials. *Mol. Simul.* **2006**, *32*, 1179−1185.
(40) Chen, R. J.; Zhang, Y.; Wang, D.; Dai, H. Noncovalent sidewall functionalization of single-walled carbon nanotubes for protein immobilization. *J. Am. Chem. Soc.* **2001**, *123*, 3838−3839.
(41) Zheng, M.; Jagota, A.; Semke, E. D.; Diner, B. A.; McLean, R. S.; Lustig, S. R.; Richardson, R. E.; Tassi, N. G. DNA-assisted dispersion and separation of carbon nanotubes. *Nat. Mater.* **2003**, *2*, 338−342.
(42) Islam, M. F.; Rojas, E.; Bergey, D. M.; Johnson, A. T.; Yodh, A. G. High weight fraction surfactant solubilization of single-wall carbon nanotubes in water. *Nano Lett.* **2003**, *3*, 269−273.
(43) Staii, C.; Johnson, A. T.; Chen, M.; Gelperin, A. DNA-decorated carbon nanotubes for chemical sensing. *Nano Lett.* **2005**, *5*, 1774−1778.
(44) Tasis, D.; Tagmatarchis, N.; Bianco, A.; Prato, M. Chemistry of carbon nanotubes. *Chem. Rev.* **2006**, *106*, 1105−1136.
(45) Su, Q.; Pang, S.; Alijani, V.; Li, C.; Feng, X.; Mullen, K. Composites of graphene with large aromatic molecules. *Adv. Mater.* **2009**, *21*, 3191−3195.
(46) Bjork, J.; Hanke, F.; Palma, C.-A.; Samori, P.; Cecchini, M.; Persson, M. Adsorption of aromatic and anti-aromatic systems on graphene through $\pi-\pi$ stacking. *J. Phys. Chem. Lett.* **2010**, *1*, 3407−3412.
(47) Ghosh, A.; Rao, K. V.; George, S. J.; Rao, C. N. R. Noncovalent functionalization, exfoliation, and solubilization of graphene in water by employing a fluorescent coronene carboxylate. *Chem.—Eur. J.* **2010**, *16*, 2700−2704.
(48) Kim, D. W.; Kim, Y. H.; Jeong, H. S.; Jung, H.-T. Direct visualization of large-area graphene domains and boundaries by optical birefringency. *Nat. Nanotechnol.* **2012**, *7*, 29−34.
(49) Malvadkar, N. A.; Sekeroglu, K.; Dressick, W. J.; Demirel, M. C. Noncovalent mechanism for the conformal metallization of nanostructured parylene films. *Langmuir* **2010**, *26*, 4382−4391.
(50) Lonberg, F.; Meyer, R. New ground state for the Splay-Freedericksz transition in a polymer nematic liquid crystal. *Phys. Rev. Lett.* **1985**, *55*, 718−721.
(51) Srajer, G.; Lonberg, F.; Meyer, R. Field-induced first-order phase transition and spinodal point in nematic liquid crystals. *Phys. Rev. Lett.* **1991**, *67*, 1102−1105.
(52) Chevallard, C.; Clerc, M. Inhomogeneous Freedericksz transition in nematic liquid crystals. *Phys. Rev. E* **2001**, *65*, 011708.
(53) Lelidis, I.; Barbero, G. Novel surface-induced modulated texture in thick nematic samples. *Europhys. Lett.* **2003**, *61*, 646−652.
(54) Pergamenshchik, V. M.; Lelidis, I.; Uzunova, V. A. Stripe domains in a nearly homeotropic nematic liquid crystal: A bend escaped state at a nematic−smectic- A transition. *Phys. Rev. E* **2008**, *77*, 041703.
(55) Berry, G. C.; Srinivasarao, M. Rheology of nematic solutions of rodlike chains: Comparison of theory and experiment. *J. Stat. Phys.* **1991**, *62*, 1041−1058.
(56) Larson, R. G. Patterns in sheared polymeric nematics. In *Spatio-Temporal Patterns in Nonequilibrium Complex Systems*; NATO advanced research workshop; Cladis, P. E., Palffy-Muhoray, P., Eds.; Addison-Wesley: Reading, MA, 1995; p 219.
(57) Forest, M. G.; Wang, Q.; Zhou, H. Methods for the exact construction of mesoscale spatial structures in liquid crystal polymers. *Physica D* **2001**, *152−153*, 288−309.
(58) Tabirian, N. V.; Nersisyan, S. R.; Kimball, B. R.; Steeves, D. M. Fabrication of high efficiency, high quality, large area diffractive waveplates and arrays. U.S. Patent 20,130,236,817, Sep 12, 2013.